The Journal of Neuroscience, May 1994, 14(5): 2933–2942

Hippocampal Reflected Optical Patterns during Sleep and Waking States in the Freely Behaving Cat

Gina R. Poe,[1] David M. Rector,[1] and Ronald M. Harper[1,2]

[1]Brain Research Institute and [2]Department of Anatomy and Cell Biology, University of California at Los Angeles, Los Angeles, California 90024-1763

We examined reflected light as a measure of neural activity from a 2 mm² area of dorsal hippocampus and surrounding neocortex in nine freely behaving cats during sleep and waking states. Light reflectance at 660 or 700 nm was measured by a coherent fiber optic probe attached to a charge-coupled device video camera that allowed acquisition of images from subcortical structures. In the dorsal hippocampus, rapid eye movement sleep (REMS) and active waking (AW) resulted in a significant decline (−0.9% ± 0.3 and −2.0% ± 0.5, respectively) in overall reflected light from the dorsal hippocampus relative to quiet sleep (QS), while quiet waking (QW) resulted in an overall increase (+2.0% ± 0.4). In the neocortical probe placement group, reflectance also decreased during AW (−1.6% ± 0.5) and increased during QW (+1.7 ± 0.6) as compared to QS. In contrast to the hippocampus, however, overall reflectance increased, rather than decreased, in the neocortex during REMS (+2.7% ± 1.3). We interpret a decline in reflectance as representing increased activation of underlying neural tissue. Thus, the cat dorsal hippocampus increased overall activity during REMS as compared to QS, while neocortical structures decreased overall activity during the same state. These results concur with expected activity changes based on electrophysiologic and autoradiographic studies. The imaging procedure provided a continuous assessment of spatially organized neural activity changes in the freely behaving animal.

[Key words: hippocampus, optical imaging, state, sleep, extracellular volume fraction, cell swelling, neocortex]

Hippocampal neurons exhibit specific activity patterns across sleep–waking states. Understanding the nature of these changes is important for assessment of state-related phenomena, including seizure threshold changes in limbic structures (Leib et al., 1980; Kellaway, 1985), state-dependent movement control (Vanderwolf, 1969, 1988), and alterations in respiratory and cardiac patterning (Komisaruk, 1970). We studied the simultaneous activity of a large number of neurons in the dorsal hippocampus of freely behaving animals to determine overall levels of state-mediated neural activity.

March 22, 1993; revised Oct. 28, 1993; accepted Nov. 1, 1993.

This research was supported by HL-22418. G.R.P. is supported by a Howard Hughes Medical Institute predoctoral fellowship. D.M.R. is supported by predoctoral fellowship NIDR DE 07212. We thank Douglas Nitz and Helen Tang for assistance.

Correspondence should be addressed to Ronald M. Harper, Ph.D., Department of Anatomy and Cell Biology, University of California at Los Angeles, Los Angeles, CA 90024-1763.

The study of neuronal activity has classically been accomplished using single neuron and gross electrical recordings. Electrophysiological studies of the dorsal hippocampus show increased overall neuronal activity during rapid eye movement sleep (REMS) and active waking (AW) compared to quiet sleep (QS) (Harper, 1971; Ranck, 1975; Suzuki and Smith, 1985; Bland and Colom, 1988; Mushiake et al., 1988; Kodama et al., 1989). However, simultaneous recording of multiple neurons for the examination of neuronal pattern interactions is arduous, and measures relationships only between relatively few neurons (typically, fewer than 10). Thus, clusters of neural discharge patterns are difficult to ascertain with electrophysiological methods.

Visualization of cell activity has been accomplished with autoradiographic and positron emission tomography (PET) studies. Glucose utilization in the hippocampus increases during REMS and waking as compared to QS (Ramm and Frost, 1986; Maquet et al., 1990). However, PET studies are limited in their ability to resolve changes across short periods of time, which leads to difficulty in resolving activity patterns in behavioral states of brief duration. In addition, autoradiography requires tissue fixation for analysis, disallowing analysis of activity variations within a state or comparison between states in the same subject.

Recently developed optical techniques can resolve patterns of neural activity, revealing the functional architecture of a region. Voltage-sensitive dyes, for example, are used to measure voltage changes across the membrane in cells and isolated nerves *in vitro* (Cohen and Lesher, 1986; Bonhoeffer and Staiger, 1988), from groups of cells in intact, restrained preparations (Grinvald et al., 1984), and from groups of cells in intact, behaving invertebrates (London et al., 1987). Dye preparations are useful for assessing short-term changes in membrane potential; however, dyes can be toxic when used repeatedly in chronic preparations that survive several months.

Light-scattering imaging techniques, which measure reflected, refracted, or transmitted light without the use of dyes, are more appropriate for chronic recordings. The wavelength measured in light scattering recordings dictates the specific cellular or vascular activities that can be assessed. Thus, different sources of light reflectance changes, such as protein conformation, blood volume, and cell volume variations, can be distinguished by appropriate wavelength selection. In addition, several activity-related processes have disparate time courses. Glial cell swelling (Kimelberg and Frangakis, 1985; Walz and Hinks, 1985) and increases in blood volume following heightened neural activity (Frostig et al., 1990) occur over a few seconds, while neuronal cell volume (Tasaki and Byrne, 1992) and protein conformation

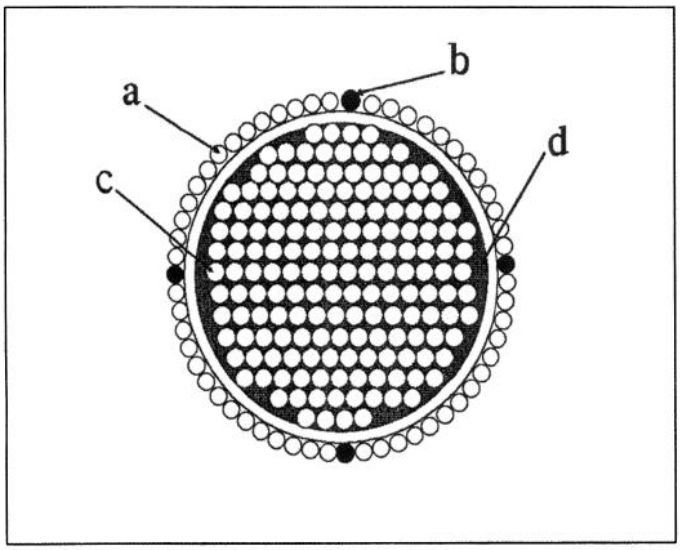

Figure 1. Schematic drawing of a cross section of 1.6-mm-diameter optic probe. The probe is surrounded by flexible optic fibers for tissue illumination (*a*). Four macroelectrodes record hippocampal or cortical EEG (*b*). The image conduit consists of at least 10,000 individual fibers. Each fiber is either 4 μm (high-resolution conduit) or 10 μm in diameter (*c*), encased by glass cladding of 1 μm (*d*), which prevents cross talk between fibers.

changes (Landowne, 1992), which are usually associated with action potentials, develop on the order of milliseconds. We measured scattered light (660 or 700 nm), which is principally affected by neural and glial volume variations between states and incorporates both fast (milliseconds) and slow (seconds) processes.

Previous investigations of light scattering in the visual cortex recorded clusters of neural activity and defined columnar structures in intact, restrained preparations (Grinvald et al., 1986; Frostig et al., 1990; Ts'o et al., 1990). Light-scattering imaging techniques also revealed coherence between reflected light and EEG amplitudes from the dorsal hippocampus of the freely behaving cat (Rector et al., 1992). Thus, the technique used in the present study can assess neural activity patterns with high temporal resolution in the freely behaving animal, and sample activity changes over extended periods of time.

Despite the well-organized disposition of cells within the hippocampus (Amaral and Witter, 1989), and the topographical organization of afferents and efferents (Ikeda et al., 1989; Tamamaki and Nojyo, 1990), few experiments describe the activity of neighboring neuronal groups in the intact dorsal hippocampus. We used a 1.6-mm-diameter fiber optic probe to transmit a coherent image from the surface of the dorsal hippocampus to a charge-coupled device (CCD) video camera. We compared reflected light levels across behavioral states in the freely behaving cat to study the simultaneous activity patterns of dorsal hippocampal neurons over naturally occurring sleep–waking states. Measurements of the surrounding neocortex display different electrophysiological patterns during REMS and AW, and served as a reference for comparison of state-related activity in the dorsal hippocampus.

Materials and Methods

Optical recording device

The imaging device, which used a coherent optic probe and miniaturized video camera, has been described elsewhere (Rector and Harper, 1991; Rector et al., 1993). Light at 660 or 700 nm wavelength was conducted from a light-emitting diode (LED) to the target tissue, either through the probe cladding or through separate optic fibers surrounding the image conduit. Reflected light traveled through 6- or 12-μm-diameter (with cladding) fibers bundled into a 1.6-mm-diameter coherent image conduit (Fig. 1). The fibers of the conduit had a 5° acceptance range for light traveling perpendicular to the plane of the probe tip. The image conduit was directly coupled to a 128-by-128 pixel CCD, where each sensing element was 25 μm in diameter and gathered light from a 650 μm^2 area. Thus, we achieved a fiber-to-pixel ratio of at least 2:1. The signal-to-noise ratio of the CCD camera was 54 dB (500:1).

Surgical procedures

Studies were carried out on nine adult cats (six female and three male) 2.8–4.0 kg in weight. Under sodium pentobarbital anesthesia, four sets of insulated, multistranded, stainless steel wires (Cooner Wire, Chatsworth, CA) were placed into the lateral costal diaphragm to determine electrocardiographic (ECG) activity. Electromyographic (EMG) activity related to inspiratory efforts was recorded from the same leads placed in the diaphragm. Cortical surface electrical activity was assessed by a pair of screw electrodes placed over the sensorimotor cortex, and neck muscle activity was recorded by flexible wires placed into the nuchal musculature. Eye movements were recorded from two screw electrodes placed in the posterior section of the orbital plate accessed through the frontal sinus. Hippocampal electroencephalographic (EEG) activity contralateral to the optic probe was recorded through a bipolar electrode (coordinates A4.0, L6.5, H9.0; Berman, 1968). Leads from four EEG macroelectrodes surrounding the optic probe were led to a nine-pin connector. The remaining electrophysiological recording electrodes were led subcutaneously to a 20-pin connector. Both connectors were attached to the surface of the skull with stainless steel screws and dental acrylic.

The optical recording device was stereotaxically positioned and fixed on the alveus of the CA1/CA2 border of the right dorsal hippocampus (A2.5, L8.0, H8.5; Berman, 1968) in five cats, approximately 2 mm deep to the surface of the suprasylvian cortex (three cats), and in the lateral temporal cortex (one cat) (Fig. 2). A 3-mm-diameter column of tissue above the probe was removed by aspiration prior to probe insertion. The skull was sealed around the probe with bone wax and dental cement to minimize movement artifact during later recording. Probe placement was verified postmortem with histological procedures. Recordings obtained after 2 weeks following postsurgical recovery were discarded for two animals whose histological analyses revealed signs of gliosis (Fig. 2*B*). Data collected during the first 2 weeks were further compared to those obtained from subjects without signs of gliosis, to ascertain that distribution patterns lay within valid range for statistical analysis.

General recording procedures

Following recovery from surgery, the animals were habituated to a sound-attenuated 1 m^3 recording chamber maintained at room temperature (approximately 22°C). This chamber was designed to allow recording from unrestrained animals. Food and water were available for consumption ad lib. Experiments began 1 week after surgery. Data were collected approximately every other day for a maximum of 10 d per cat. During each recording, the animals were allowed to sleep undisturbed for at least two complete sleep–waking cycles.

State classification

Sleep and waking states were scored according to standard electrophysiological criteria (Ursin and Sterman, 1981), including cortical and hippocampal EEG, neck muscle tonus, and eye movements. Active waking (AW) and rapid eye movement sleep (REMS) were both characterized by rhythmical slow activity (4–9 Hz) in the hippocampal EEG, desynchronized neocortical EEG, and rapid eye movements. We selected epochs of REMS with muscle atonia, whereas muscle tonus was high and variable during AW. Epochs with overt rhythmicity in fluctuation of neck muscle tone and eye movement were not included in the analysis to exclude grooming and eating behaviors from AW. Periods of quiet waking (QW) were defined by low-voltage, desynchronized hippocampal and neocortical EEG, high-amplitude neck muscle tone without fluctuation, and eyes open as measured through the electrooculogram. Feline stage 2 sleep (QS), characterized by continuous, large-amplitude slow waves (0–1.5 Hz) intermixed with 12–14 Hz spindle

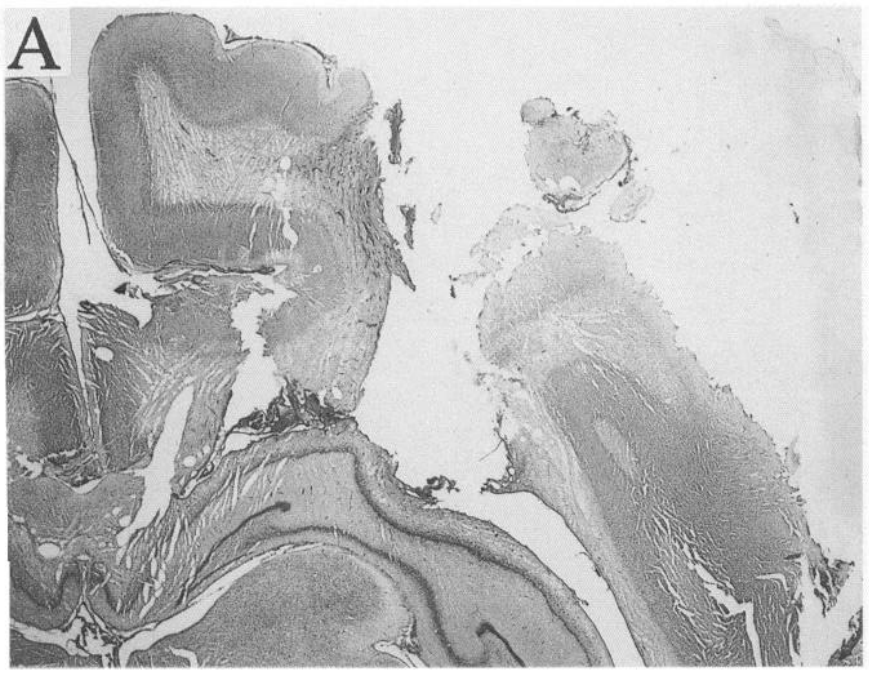

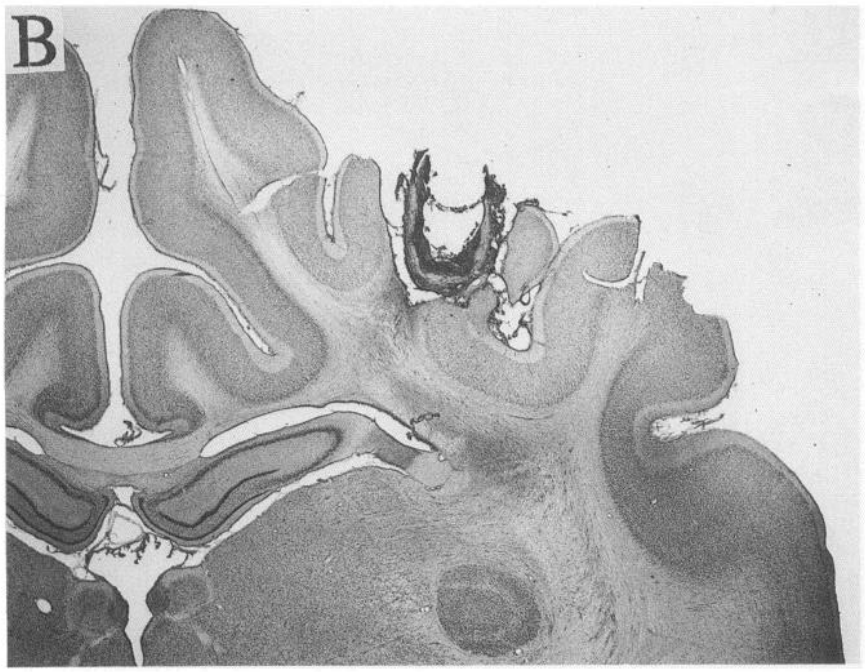

Figure 2. Histology: representative 60 μm slices of brain tissue from a probe placement site in the hippocampus (*A*), and in the neocortex (*B*). Slices were stained for neuronal cell bodies with Nissl blue.

activity in the neocortical and hippocampal EEG, as well as minimal eye movements and intermediate muscle tone, was used as the reference for state comparisons to AW, QW, and REMS. Changes in state between active and quiet waking occurred rapidly (<1 sec), and thus, to achieve stable recording conditions and for ease of state scoring, a minimum state duration for acquisition of 15 frames (45 sec) was used. To ensure a "natural" sleep–waking cycle, no experimental manipulations, such as sleep deprivation or external arousal, were employed. Thus, any single state may not have been present for sufficient duration in a recording period for adequate analysis. To collect a sufficient sample of all states, each cat was studied over several recording periods.

Optical and electrophysiological acquisition procedures

Video output of the CCD array was amplified, digitized by an eight-bit framegrabber, and stored on a computer. To maximize the dynamic range of the digitizer (discussed in Inoue, 1986), the LED voltage was set before each experiment to two-thirds the maximal reflectance amplitude, the black level (0) was set to approximately one-half the amplitude of the minimal pixel value, and the gain on the amplifier was set so that the maximal amplitude pixel was represented by a value of approximately three-quarters of a 0–255 range. The framegrabber was triggered to read any frame in 1/60 sec through computer logic that

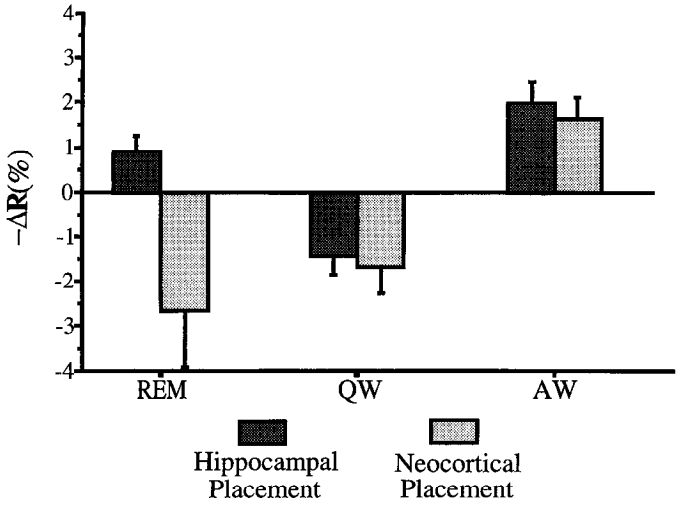

Figure 3. Overall activity changes. The histogram illustrates the overall state-dependent change in activity expressed as the negative percentage change in reflectance from baseline (QS) reflectance levels. Data were normalized and averaged across all animals from hippocampal and neocortical placement sites.

sensed a pulse initiated by the cardiac R wave. Sampling of frames relative to the timing of the cardiac pulse minimized potential movement artifact from cardiovascular sources. Transfer of a frame to the computer was accomplished over a 3 sec time period, after which a new scan was initiated. This transfer rate was sufficient to resolve activity patterning changes between sleep–waking states. The video signal was also stored on S-VHS video tape at a continuous frame rate (60 noninterlaced frames/sec). Concurrent electrophysiological activity (including electrical activity from recording electrodes attached to the fiber bundle) was bandpass filtered (ECG, 1–100 Hz; EMG, 10 Hz to 1 kHz; EEG, 0.1–40 Hz), written onto polygraph paper, and stored as a multiplexed signal on the videotape audio channels. Electrophysiological signals were also digitized and stored on a separate computer at appropriate rates according to Nyquist frequency guidelines.

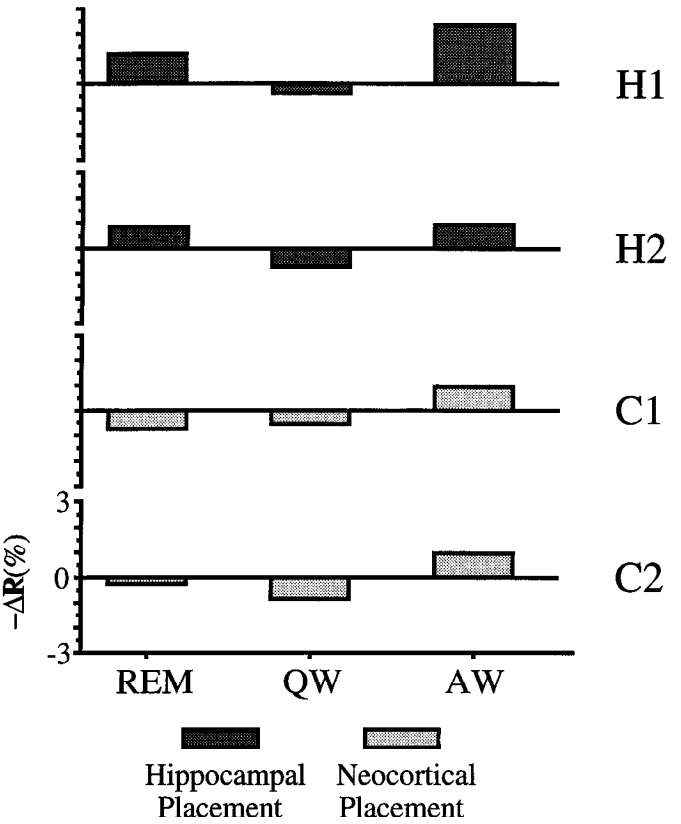

Figure 4. Single experiment activity changes: histogram. The histogram illustrates the state-dependent change in activity from four different sleep–wake cycles in four separate cats: hippocampal probe-placement cats (*H1, H2*), and neocortical probe-placement cats (*C1, C2*). Activity is expressed as the negative percentage change in reflectance from baseline (QS) reflectance levels. SDs of the mean never exceeded 0.01%, and, thus were not included in the histogram.

Table 1. Standard deviations: comparison between sites and states

State	Hippocampus	Neocortex
QS	0.7	1.3
REM	1.0	2.1
QW	2.2	2.4
AW	2.5	3.6
Average	1.6	2.4

Levene's test for variability within image-averaged normalized data grouped by state shows the variance between all states to be significantly different at $p < 0.0001$, with the following three exceptions: AW is significantly different from QW in the neocortex at $p = 0.01$, QW is not significantly different from REM in the neocortex ($p = 0.15$), and QW is not significantly different from AW in the hippocampus ($p = 0.7$).

Image processing

Processing of the video frames was performed on an A3000 video computer (Commodore Business Machines, West Chester, PA). Reflectance amplitude was calculated and recorded for each pixel of each image frame.

State averaging. State-averaged images were generated by calculating the average reflectance of each pixel with the same x-y coordinates from every frame gathered in a particular state. The number of frames included in the average ranged from 15 to 50, depending on the duration of the state. The image processing software utilized a 32-bit integer for internal data representation, allowing averaging of up to 16 million eight-bit images without possibility of data overflow. State-averaged images were subtracted from the mean QS image from the same sleep–waking cycle to obtain reflectance changes between states. In keeping with the precedent set by other investigations of neurally mediated optical changes (e.g., Grinvald et al., 1986), subtracted images were pseudocolored to display regional and directional activity changes for those pixels which were significantly different between conditions (ANOVA, $\alpha = 0.05$). A decrease in reflectance from baseline was displayed as a positive value, correlating with increased neural activity.

Image averaging. Average reflectance values were calculated across all pixels within each image frame. These values were then normalized, according to the following procedure, to show the negative percentage change in reflectance [$-\Delta R(\%)$], or the percentage change in activity from the baseline state. The average reflectance value of each image (R_X) within QS, REMS, AW, and QW, was subtracted from, then divided by, the mean reflectance value of all images from the baseline state (R_{QS}):

$$-\Delta R(\%) = \text{activity change } (\%) = [(R_{QS} - R_X)/R_{QS}] \times 100$$

The image-averaged normalization procedure accounted for differences in light input and gain settings between experiments, yet allowed for the full range of image-averaged reflectance variation within and between states. Normalized overall activity values were plotted over time.

Statistical analysis. An unbalanced, repeated-measures ANOVA (BMDP-5V; Dixon et al., 1990), with a restricted maximum likelihood algorithm to account for missing data points, was performed on state-averaged, normalized data to calculate the significance of the activity differences between states, experiment dates, and probe placement sites. The unbalanced, repeated-measures ANOVA was used because the composition of states within each experiment date and the number of experiments per subject varied. A general mixed-model analysis of variance (BMDP-3V) was performed using image-averaged, normalized data to estimate the mean and standard deviation of overall reflectance during each state on each experiment date. A regression analysis was

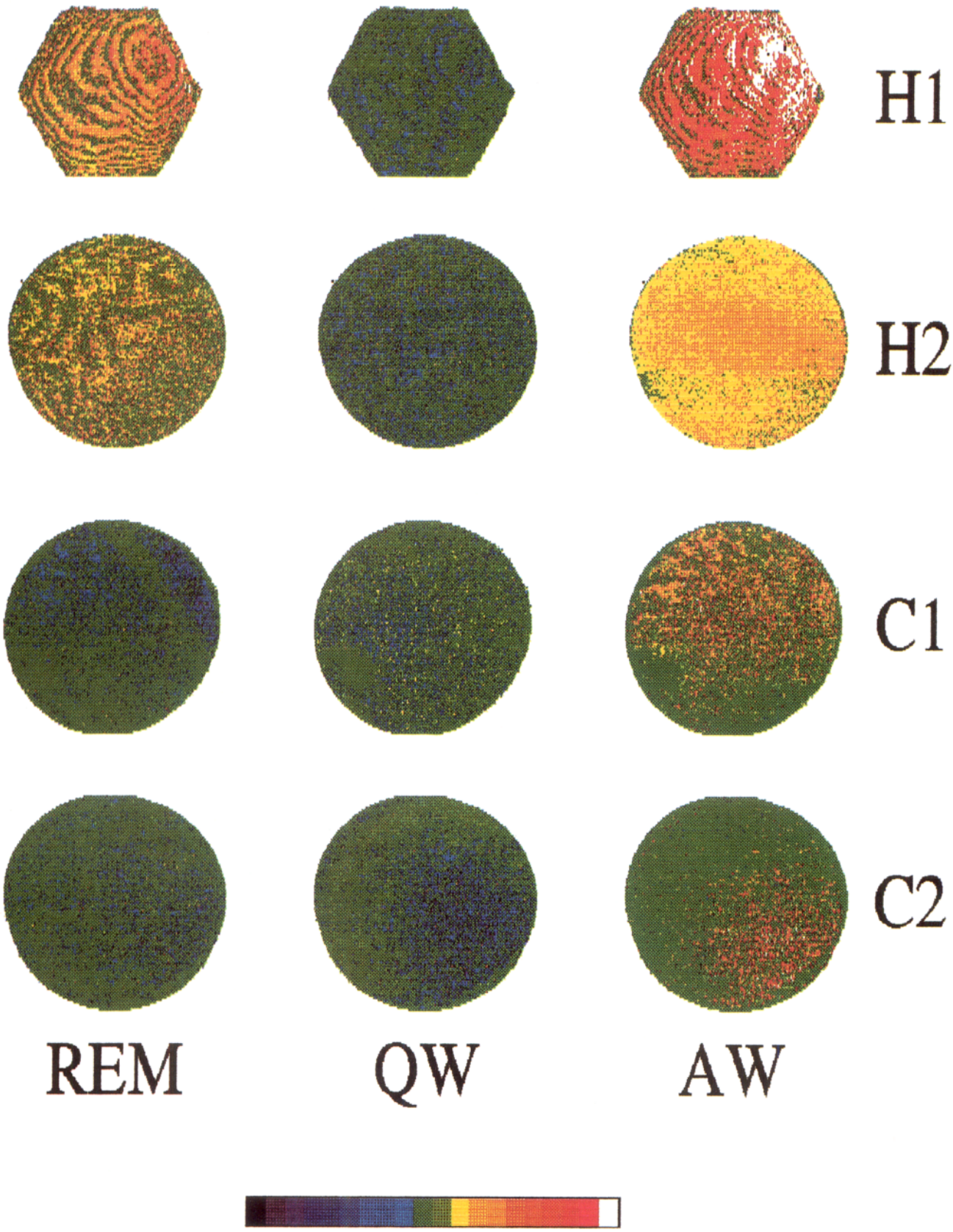

Figure 5. Single experiment activity changes: images. The same data samples used for the histograms of Figure 4 are here displayed in image form. Pixel-by-pixel differences between the state shown and QS are displayed where significant at $\alpha = 0.05$. The *color bar* in the lower portion of the figure is the pseudocolor scale used to illustrate changes in activity. *Yellow to red pixels* indicate areas of increased activity (decreased reflectance), with *white* representing an activity increase of 3.3%. *Blue to purple pixels* indicate areas of decreased activity (increased reflectance), with *black* representing an activity decrease of 3.3%. *Green pixels* indicate no significant difference in activity between the two states. Each image is approximately 1.6 mm in diameter.

performed to analyze trends in state-related activity across experiment dates, which assisted in determining whether the data gathered from the optic measurement system were consistent over extended periods of time. A Box-Cox analysis (BMDP-7D) was applied to image-averaged, normalized data to confirm normal distributions. The Levene test for data variability differences (BMDP-3D) was also applied to image-averaged, normalized data to ensure that all data were comparable, and to assess the contribution of state to variability in light reflectance. Variability calculations were also made for each state to assess the potential contribution of movement artifact to image variability.

Since the data were collected from differing numbers of experiments per cat, the mean percentage change in activity between states was determined by averaging state-grouped, normalized data across all experimental dates for each subject, followed by averaging across all subjects within each placement site.

Results

Overall state changes

Sleep–waking state significantly affected image-averaged reflectance in the hippocampus and the neocortex ($p < 0.001$). Since no significant subject effects emerged, normalized data were averaged across animals within each placement group to form the summary histogram in Figure 3. SE bars signify the variance between subjects.

Hippocampus. Optical measures of overall activity in the hippocampus increased 0.9% ± 0.3 (mean ± SE, $p < 0.04$) in REMS and 2.0% ± 0.5 ($p < 0.001$) in AW relative to QS, and declined 2.0% ± 0.4 ($p < 0.001$) during QW as compared to QS in the dorsal hippocampus.

Neocortex. Like the hippocampus, overall activity increased 1.6% ± 0.5 ($p < 0.001$) in the neocortex during AW and decreased 1.7 ± 0.6 ($p < 0.008$) during QW. However, unlike the hippocampus, overall activity decreased during REMS 2.7% ± 1.3 ($p < 0.002$), relative to QS. During REMS, the neocortical EEG was desynchronized, whereas the hippocampus displayed highly synchronous EEG patterns in the 4–9 Hz range. The amplitude and direction of reflectance change differed between the hippocampus and neocortex only for the REMS-QS comparison ($p < 0.004$), as demonstrated in Figure 3.

Activity changes between states during four representative experiments from four separate animals, are shown in Figure 4. AW and QW change similarly when comparing hippocampal to cortical placements, but REMS shows higher activity than QS in hippocampal placements and lower activity than QS in neocortical placements. The corresponding difference images in Figure 5 were obtained by subtracting REM, QW, and AW average images from a QS average image and color coding for activity change. Patterns of increased and decreased activity appeared across each image. The hippocampus consistently displayed distinct spatial patterns of stripes and bands of activity in every animal under one or more conditions; however, the neocortex showed regions of increased or decreased activity that usually formed patches, rather than bands.

Variability influences

The variability of image-averaged normalized reflectance values between states is described in Table 1. We took substantial precautions to minimize reflectance variations induced by brain movements by using a closed-skull preparation and by time-locking image acquisitions to the cardiac pulse. Additionally, four EEG macrowires extended beyond the probe and restrained tissue movement. As shown in Table 1, brain movements were not the principal contributing factor to image variability within states. For example, overall image-to-image reflectance variability in the hippocampus, as calculated by Levene's test, did not significantly differ ($p = 0.7$) between QW (without movements) and AW (with high muscle tonus and movements). We selected REMS epochs with muscle atonia and without phasic myoclonus. REMS showed higher signal variability than QS ($p < 0.001$), indicating that muscle activity or movements did not significantly contribute to image variability.

The hippocampus exhibited less image-averaged overall variability than the neocortex ($p < 0.001$), as is demonstrated by the average SD calculated for each placement site (Table 1) and by the time series plot of image-averaged, normalized activity changes (Fig. 6). The time course traces in Figure 6 are samples of activity changes within states. For example, the dip in activity during QW in Figure 6*A* does not always occur in the early portion of the state or for the precise duration shown. However, the overall trends and the within-state image variability are typical of each probe placement group. Overall activity increased in the hippocampus (Fig. 6*A*) during REMS but decreased in the neocortex (Fig. 6*B*), as was seen in the images of Figure 5.

Trends in state-specific activity differences across experiment dates are plotted in Figure 7. This figure demonstrates that significant differences in activity occur between experimental dates. Note, however, that the relationship between states remains intact within each probe placement group. Thus, in Figure 7*A* (hippocampus), REMS and AW traces show higher activity levels than the QS trace over experimental dates, despite variations in the exact percentage of activity increase between experiments. The relationship between QW and QS activity levels was more variable in the hippocampus, but either the difference did not attain statistical significance (dates 1, 3, and 8) or QW was significantly less active than QS. Figure 7*B* (neocortex) also shows variations in activity levels within each state across dates, but again, the activity level relationship between each state and QS was consistent across dates. REMS and QW both displayed lower activity than QS across experiments, and AW exhibited increased activity levels. Although significant activity differences occurred between dates, regression analyses of the activity in each state across dates (Table 2) revealed that no significant positive or negative trend in activity occurred across experiment dates ($p = 0.24$ and 0.15 in the hippocampus and neocortex, respectively).

Histology

Among the hippocampal placements, all probes were within 1 mm of the dorsal hippocampal surface illustrated in Figure 2*A* in rostrocaudal and mediolateral planes, and all probes rested on the alveus in the CA1/CA2 border region. In both hippocampal and neocortical placements, positions were unchanged from one experiment to the next in the same cat, since the probes were cemented in place, and no evidence of displacement was found on histological examination.

Discussion

Sleep–waking states produced reliable activity changes in the dorsal hippocampus that were distinct from the neocortex. REMS produced an overall rise in activity relative to QS in the hippocampus, but produced a decline in activity relative to QS in the neocortex. Activity changes of a similar direction and amplitude occurred in the hippocampus and the neocortex during AW (activity rise) and QW (activity decline) compared to QS.

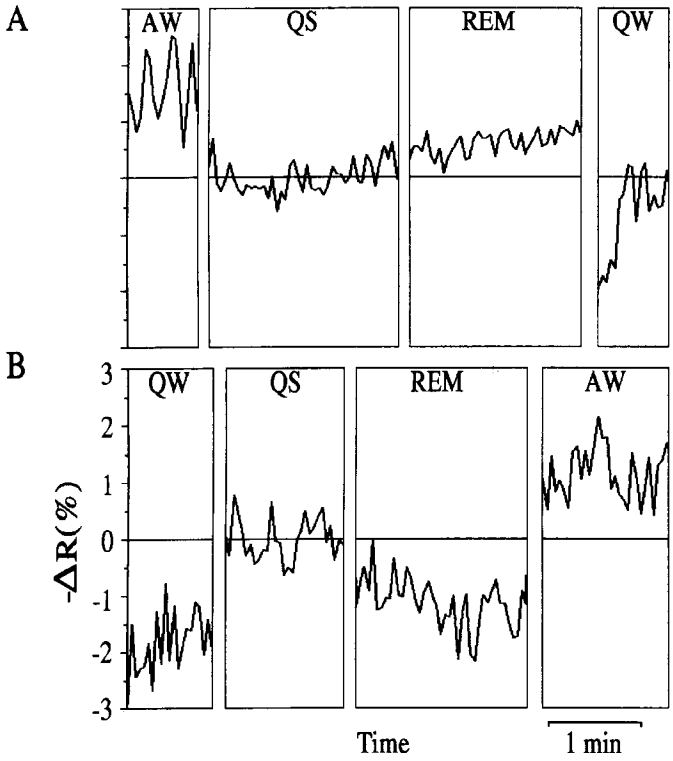

Figure 6. Time series analysis of image-averaged normalized data. *A* shows image-averaged activity changes (negative percentage change in reflectance) of sequential frames, during an experiment where the optic probe rested on the dorsal hippocampus. States, indicated above the traces, occurred in the order indicated. Transitions and/or other states unexamined in this study occurred between the states and, for the sake of clarity, are not shown. *B* indicates activity changes in images gathered from the suprasylvian cortex overlying the dorsal hippocampus.

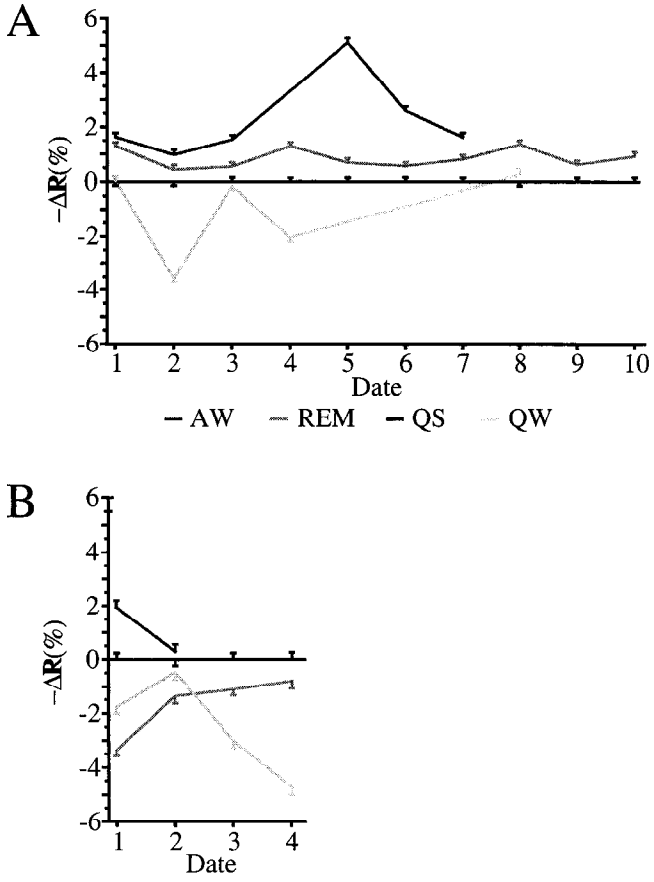

Figure 7. State-dependent activity over experiments: estimation of the mean and SE of overall state-dependent activity (negative change in reflectance) from the dorsal hippocampus on each experiment date for each placement group. *A*, Hippocampus; up to 10 experiments were completed on each animal. Typically, experiments from at least four cats were averaged per date, except day 10, when data from one cat were entered. *B*, Neocortex; a maximum of four experiments were completed on each animal. Experiments from at least three cats were averaged for all dates except day 4, when data from one subject contributed to the estimate.

Greater image-to-image variability (Fig. 6, Table 1) was observed in the neocortex compared to the dorsal hippocampus, although the hippocampus exhibited more distinct pattern differentiation (Fig. 5).

Reflectance—physical properties

Amaral and Witter (1989) and Tamamaki and Nojyo (1990) suggest slab-like modules of 0.3–0.6 mm in diameter in the dorsal hippocampus. Thus, if the spatial organization of the tissue is preserved through the recording procedure, the 1.6-mm-diameter probe would be sufficient to resolve such structures. Since the fiber optic probe does not use a lens, and the illuminating and light-capturing fibers of the probe have a 5° light emission/acceptance range, the tissue components closest to the probe tip are in sharpest focus. However, each pixel represents light scattering from a volume of tissue beneath the probe. Investigation of the light scattering properties of the dorsal hippocampus and neocortex are currently underway to assess the resolution characteristics of the probe and numbers of neural elements contributing to the reflectance value of each pixel.

Several lines of evidence suggest that the banding patterns observed in the hippocampus represent neural phenomena rather than artifact acquired during image gathering or processing. The image processing software used sufficiently large integers in the arithmetic calculations (32 bit) to eliminate possibility of data overflow when averaging 50 images. In addition, banding patterns were found in the hippocampus, but not in the neocortex when identical image processing and acquisition techniques were employed. The banding patterns changed between behaviors from the same animal during the same experiment, where all images were treated with the same signal acquisition and processing techniques. Lastly, patches, rather than bands of enhanced or decreased reflectance were found in a study using similar acquisition and processing techniques on the ventral medullary surface (Dong et al., 1993; Gozal et al., 1993), where histological projection patterns would not anticipate the functional bands or lamellae that are found in the hippocampus. A detailed mapping of dorsal hippocampal activity patterns will be the subject of future studies.

Reflectance—neural activity correlates

We interpret a decline in reflectance to indicate a rise in neural activity, and a rise in reflectance to indicate a decline in neural activity. We observed a decline in 660 nm light reflectance in the dorsal hippocampus upon intrahippocampal glutamate administration through a microdialysis probe in the freely behaving animal (G. R. Poe, D. M. Rector, and R. M. Harper, unpublished observations), and after Schaeffer collateral stimulation (Rector et al., 1993). Similar reflectance changes corresponding

Table 2. Regression analysis of activity over experiments

	State	*r*	*p*
Hippocampus	QS	0.00	1.00
	REM	0.03	0.95
	QW	0.32	0.60
	AW	0.30	0.56
Neocortex	QS	0.00	1.00
	REM	0.89	0.11
	QW	0.81	0.19
	AW	1.00	—

Data are from regression analysis of activity trends across experiment dates shown in Figure 7. QS analyses are based on observed data, as there were no missing values. Other regression calculations were based on predicted means, as described in Materials and Methods.

to levels of neural activity were observed during *in vivo* optical mapping of visual cortex ocular dominance columns (Grinvald et al., 1986).

Several mechanisms potentially underlie the reflectance phenomena observed, including blood perfusion, protein conformation, and cell volume changes. Although variations in blood flow and volume accompany neural discharge, the optical patterns are unlikely to result solely from blood perfusion dynamics. Frostig et al. (1990), studying blood perfusion and neuronal activity in the cat visual cortex, found that longer wavelengths (red/infrared) optimally correlate to neural activity, and shorter wavelengths (green/orange) better demonstrate changes in blood flow. Light absorption from blood is maximal at 570 nm (Perkampus, 1971), rather than at 660 and 700 nm, the wavelengths used in our studies. In the blood-free preparation, protein conformation changes that accompany neural activity are optimally measured in the ultraviolet range (280–350 nm) (Landowne, 1992). MacVicar and Hochman (1991), using the blood-free preparation of the *in vitro* hippocampal slice, found that 700 nm light transmission increased when neural activity increased following stimulation of Schaeffer's collaterals. After using a succession of ionic blockades to alter flow across membranes, they hypothesized that increased neural discharge results in cell swelling, causing increased light transmission. A recent study by Tasaki and Byrne (1992) demonstrated that rapid swelling and shrinking of nerve fibers upon stimulation occurred on the time order of action potentials. They showed that displacement of the nerve surface, an increase in the pressure exerted by the nerve surface, and a reduction of reflected light intensity all occur in conjunction with an increase in water content upon electrical stimulation of the fibers.

The hypothesis that neural tissue swells when neurons discharge is further supported by studies relating intracellular and extracellular volume to neural discharge levels. Neural activity in the CA1 region of the hippocampal slice inversely relates to the extracellular volume fraction (McBain et al., 1990). Increased synchronous firing accompanies shrinkage of extracellular space even when synaptic transmission is blocked (Taylor and Dudek, 1984a,b; Dudek et al., 1990; Roper et al., 1992). Cohen and Keynes (1971) suggested that cell swelling accompanying ionic exchanges during the action potential reduces the refractive index of the intracellular fluid toward that of the extracellular fluid. Therefore, when the cell swells, decreased light reflects from the cell surface, and increased light is either transmitted or absorbed by intracellular elements. Thus, state-related changes in discharge frequency and synchrony could account for the reflectance changes observed in the dorsal hippocampus and neocortex.

State findings—hippocampus

REMS and AW. Functional mapping of brain regions that are active during specific sleep states can assist the determination of relationships of particular structures to the initiation, maintenance, or participation in sleep states. Measurements of glucose utilization using PET in the human (Maquet et al., 1990) and autoradiographic studies in the cat (Ramm and Frost, 1986) reveal decreased glucose utilization in the hippocampus during QS than during both REMS and waking. This result supports our finding that reflectance measurements of neural activity decrease during QS as compared to REMS and AW. The temporal resolution restrictions of glucose utilization studies, however, preclude the subclassification of levels of waking vigilance that we have found to be critical when comparing AW versus QW to QS.

Electrophysiological unit recording studies also find increased activity in the dorsal hippocampus during REMS and AW compared to QS. A set of granule cells and interneurons lying above the pyramidal layer (Fox and Ranck, 1975) are three to four times more active in REMS than in QW and QS (Ranck, 1975; Suzuki and Smith, 1985). Complex-spiking pyramidal cells fire most frequently during QS. However, their firing frequencies are from 50 to 600 times below those of interneurons during QS, AW, and REMS. Thus, the highest activity levels observed during AW and REMS appear to result primarily from increased synchronous firing of interneurons.

Quiet waking. During QW, reflectance measurements indicate that overall hippocampal activity declined as compared to QS. Studies of unit discharge in this region reveal that both complex-spiking pyramidal cells and interneurons reduce discharge frequency during the low-voltage asynchronous activity associated with QW as compared to QS (Ranck, 1973; Suzuki and Smith, 1985; Mushiake et al., 1988; Kodama et al., 1989). Thus, hippocampal electrophysiological data support the change in activity during QW observed through measurements of reflectance patterns.

State findings—neocortex

Active and quiet waking. Over most regions of the brain, PET and autoradiographic studies (Kennedy et al., 1982; Ramm and Frost, 1986; Maquet et al., 1990) detect an increase in glucose utilization during waking as compared to QS. However, certain cortical regions, such as parietal (Maquet et al., 1990) and suprasylvian areas (Ramm and Frost, 1986), show a mixed or decreased level of activity during waking compared to QS. Again, these studies do not subclassify the waking states (QW vs AW), which are significant in our comparisons to QS. We would predict that neural activity during AW would slightly increase as compared to QS, but decrease during QW. Indeed, electrophysiological studies of fast-conducting pyramidal neurons in the neocortex, which constitute the majority of neocortical pyramidal cells, report that firing rates decrease to near zero levels during aroused waking without movement (Steriade et al., 1974), and the discharge rate of nonpyramidal neurons declines during QW to almost half their discharge rate during QS (Evarts, 1964; Steriade et al., 1974). Our findings indicate a decrease in activity during QW as compared to QS.

REM sleep. Autoradiographic and PET studies find increased glucose utilization during REMS compared to QS in the neo-

cortex (Kennedy et al., 1982; Ramm and Frost, 1986; Maquet et al., 1990), which would appear to be inconsistent with our finding that activity decreased during REMS as compared to QS. However, using optical transmission techniques at near-infrared (780, 805, and 830 nm) wavelengths, Hayaishi and colleagues (Hayaishi, 1990; Onoe et al., 1991) found that another correlate of neural activity, deoxyhemoglobin levels, decreased while oxyhemoglobin levels increased in frontal neocortical circulation during REMS compared to QS and waking. They suggest that frontal neocortical neurons may be less active during REMS as compared to QS and waking. Our results also indicate decreased activity during REMS in the neocortex proximal to the hippocampus.

Discharge rates in neocortical neurons vary as a function of cerebral area as well as specific state. The diversity of cell groups sampled within the neocortex defy a collective statement on reflective properties appropriate for overall assessment of cortical regions. Instead, we emphasize that cortical regions surrounding the hippocampus apparently reflect light differently than the hippocampus during comparable behavioral states.

Dynamic patterns

Examination of moment-to-moment reflectance values revealed substantial fluctuations over time. Since we sampled reflectance at 2.5–3 sec intervals, relationships of reflectance to more rapidly changing events, such as the EEG, are not possible. However, the moment-to-moment variations in reflectance amplitude most likely represent underlying changes in neural activity within states. Indeed, when images were gathered at higher sampling rates (Rector et al., 1992), the spectral compositions of EEG and image amplitudes were nearly superimposable.

Summary

Activity measurements of multiple neurons from the freely behaving cat show that the dorsal hippocampus and neocortex display differing state-dependent activity patterns. Optical measures of neural activity can be assessed in freely behaving animals to reveal spatially preserved activity patterns of large groups of neurons within and between naturally occurring sleep–waking states.

References

Amaral DG, Witter MP (1989) The three-dimensional organization of the hippocampal formation: a review of anatomical data. Neuroscience 31:571–591.

Berman A (1968) The brain stem of the cat. Madison, WI: University of Wisconsin.

Bland BH, Colom LV (1988) Responses of phasic and tonic hippocampal theta-on cells to cholinergics: differential effects of muscarinic and nicotinic activation. Brain Res 440:167–171.

Bonhoeffer T, Staiger V (1988) Optical recording with single-cell resolution from monolayered slice cultures of rat hippocampus. Neurosci Lett 92:259–264.

Cohen LB, Keynes RD (1971) Changes in light scattering associated with the action potential in crab nerves. J Physiol (Lond) 212:259–275.

Cohen LB, Lesher S (1986) Optical monitoring of membrane potential: methods of multisite optical measurement. In: Optical methods in cell physiology (DeWeer P, Salzberg BM, eds), pp 71–99. New York: Wiley.

Dixon WJ, Brown MB, Engelman L, Jennrich RI, eds (1990) BMDP statistical software manual. Los Angeles: University of California.

Dong XW, Gozal D, Rector DM, Harper RM (1993) Ventilatory CO_2-induced optical activity changes of cat ventral medullary surface. Am J Physiol 265:R494–R503.

Dudek FE, Obenaus A, Tasker JG (1990) Osmolality-induced changes in extracellular volume alter epileptiform bursts independent in chemical synapses in the rat: importance of non-synaptic mechanisms in hippocampal epileptogenesis. Neurosci Lett 120:267–270.

Evarts EV (1964) Temporal patterns of discharge of pyramidal tract neurons during sleep and waking in the monkey. J Neurophysiol 27: 152–171.

Fox SE, Ranck JB Jr (1975) Localization and anatomical identification of theta and complex-spike cells in dorsal hippocampal formation of rats. Exp Neurol 49:299–313.

Frostig RD, Lieke EE, Ts'o DY, Grinvald A (1990) Cortical functional architecture and local coupling between neuronal activity and the microcirculation revealed by *in vivo* high-resolution optical imaging of intrinsic signals. Proc Natl Acad Sci USA 87:6082–6086.

Gozal D, Dong XW, Rector DM, Harper RM (1993) Optical imaging of the ventral medullary surface of cats: hypoxia-induced differences in neural activation. J Appl Physiol 74:1658–1665.

Grinvald A, Anglister L, Freeman JA, Hildesheim R, Manker A (1984) Real-time optical imaging of naturally evoked electrical activity in intact frog brain. Nature 308:848–850.

Grinvald A, Lieke E, Frostig RD, Gilbert CD, Wiesel TN (1986) Functional architecture of cortex revealed by optical imaging of intrinsic signals. Nature 324:361–364.

Harper RM (1971) Frequency changes in hippocampal electrical activity during movement and tonic immobility. Physiol Behav 7:55–58.

Hayaishi O (1990) Oxyhemoglobin increases and deoxyhemoglobin decreases in the circulation of the brain of the rhesus monkey during REMS but not during slow wave sleep. In: Slow wave sleep: its measurement and functional significance (Chase MH, Roth T, eds), pp 36–37. Los Angeles: Brain Information Service/Brain Research Institute, University of California at Los Angeles.

Ikeda J, Mori K, Oka S, Watanabe Y (1989) A columnar arrangement of dendritic processes of entorhinal cortex neurons revealed by a monoclonal antibody. Brain Res 505:176–179.

Inoue S (1986) Video microscopy. New York: Plenum.

Kellaway P (1985) Sleep and epilepsy. Epilepsia 26[Suppl 1]:S15–S30.

Kennedy C, Gillin JC, Mendelson W, Suda S, Miyaoka M, Ito M, Nakamura RK, Storch FI, Pettigrew K, Mishkin M, Sokoloff L (1982) Local cerebral glucose utilization in non-rapid eye movement sleep. Nature 297:325–327.

Kimelberg HK, Frangakis MV (1985) Furosemide- and Bumetanide-sensitive ion transport and volume control in primary astrocyte cultures from rat brain. Brain Res 361:125–134.

Kodama T, Mushiake H, Shima K, Nakahama H, Yamamoto M (1989) Slow fluctuations of single unit activities of hippocampal and thalamic neurons in cats. I. Relation to natural sleep and alert states. Brain Res 487:26–34.

Komisaruk BR (1970) Synchrony between limbic system theta activity and rhythmical behavior in rats. J Comp Physiol Psychol 70:482–492.

Landowne D (1992) Optical activity change with nerve impulses. Biophys J 61:A109.

Leib JP, Joseph JP, Engel J Jr, Walker J, Crandall PH (1980) Sleep state and seizure foci related to depth spike activity in patients with temporal lobe epilepsy. Electroencephalogr Clin Neurophysiol 49: 538–557.

London JA, Zecevic D, Cohen LB (1987) Simultaneous optical recording of activity from many neurons during feeding in *Navanax*. J Neurosci 7:649–661.

MacVicar BA, Hochman D (1991) Imaging of synaptically evoked intrinsic optical signals in hippocampal slices. J Neurosci 11:1458–1469.

Maquet P, Dive D, Salmon E, Sadzot B, Franco G, Poirrier R, von Frenkell R, Frank G (1990) Cerebral glucose utilization during sleep–wake cycle in man determined by positron emission tomography and [^{18}F]2-fluoro-2-deoxy-D-glucose method. Brain Res 513:136–143.

McBain CJ, Traynelis SF, Dingledine R (1990) Regional variation of extracellular space in the hippocampus. Science 249:674–677.

Mushiake H, Kodama T, Shima K, Yamamoto M, Nakahama H (1988) Fluctuations in spontaneous discharge of hippocampal theta cells during sleep-waking states and PCPA-induced insomnia. J Neurophysiol 60:925–939.

Onoe H, Watanabe Y, Tamura M, Hayaishi O (1991) REM sleep-associated hemoglobin oxygenation in the monkey forebrain studied using near-infrared spectrophotometry. Neurosci Lett 129:209–213.

Perkampus HH, ed (1971) UV atlas of organic compounds, Vol V. New York: Plenum.

Ramm P, Frost BJ (1986) Cerebral and local cerebral metabolism in the cat during slow wave and REM sleep. Brain Res 365:112–124.

Ranck JB Jr (1973) Studies on single neurons in dorsal hippocampal formation and septum in unrestrained rats. I. Behavioral correlates and firing repertoires. Exp Neurol 41:461–531.

Ranck JB Jr (1975) Behavioral correlates and firing repertoires of neurons in the dorsal hippocampal formation and septum of unrestrained rats. In: The hippocampus, Vol 2, Neurophysiology and behavior (Isaacson RL, Pribram KH, eds), pp 207–244. New York: Plenum.

Rector DM, Harper RM (1991) Imaging of hippocampal neural activity in freely behaving animals. Behav Brain Res 42:143–149.

Rector DM, Poe GR, Harper RM (1992) Assessment of dorsal hippocampal optical properties concurrent with electrophysiological measures at high temporal and spatial resolution. Soc Neurosci Abstr 18:918.

Rector DM, Poe GR, Harper RM (1993) Fiber optic imaging of subcortical neural tissue in freely behaving animals. Adv Exp Med Biol 333:81–86.

Roper SN, Obenaus A, Dudek FE (1992) Osmolality and nonsynaptic epileptiform bursts in rat CA1 and dentate gyrus. Ann Neurol 31:81–85.

Steriade M, Deschenes M, Oakson G (1974) Inhibitory processes and interneuronal apparatus in motor cortex during sleep and waking. I. Background firing and responsiveness of pyramidal tract neurons and interneurons. J Neurophysiol 37:1065–1092.

Suzuki S, Smith G (1985) Single cell activity and synchronous bursting in the rat hippocampus during waking behavior and sleep. Exp Neurol 89:71–89.

Tamamaki N, Nojyo Y (1990) Disposition of slab-like modules formed by axon branches originating from single CA1 pyramidal neurons in the rat hippocampus. J Comp Neurol 291:509–519.

Tasaki I, Byrne PM (1992) Rapid structural changes in nerve fibers evoked by electrical current pulses. Biochem Biophys Res Comm 188: 559–564.

Taylor CP, Dudek FE (1984a) Excitation of hippocampal pyramidal cells by an electrical field effect. J Neurophysiol 52:126–142.

Taylor CP, Dudek FE (1984b) Synchronization without active chemical synapses during hippocampal afterdischarges. J Neurophysiol 52: 143–155.

Ts'o DY, Frostig RD, Lieke EE, Grinvald A (1990) Functional organization of primate visual cortex revealed by high resolution optical imaging. Science 249:417–420.

Ursin R, Sterman MB (1981) A manual for standardized scoring of sleep and waking states in the adult cat. Los Angeles: Brain Information Service/Brain Research Institute, University of California at Los Angeles.

Vanderwolf CH (1969) Hippocampal electrical activity and voluntary movement in the rat. Electroencephalogr Clin Neurophysiol 26:407–418.

Vanderwolf CH (1988) Cerebral activity and behavior: control by central cholinergic and serotonergic systems. Int Rev Neurobiol 30: 225–340.

Walz W, Hinks E (1985) Carrier-mediated KCl accumulation accompanied by water movements is involved in the control of physiological K^+ levels by astrocytes. Brain Res 343:44–51.